Published in final edited form as:
J Cardiovasc Transl Res. 2011 August ; 4(4): 493–503. doi:10.1007/s12265-011-9284-0.

From Molecules to Myofibers: Multiscale Imaging of the Myocardium

Craig J. Goergen and
Martinos Center for Biomedical Imaging, Massachusetts General Hospital, Harvard Medical School, Boston, MA, USA

David E. Sosnovik
Martinos Center for Biomedical Imaging, Massachusetts General Hospital, Harvard Medical School, Boston, MA, USA. Cardiology Division, Massachusetts General Hospital, Harvard Medical School, Boston, MA, USA. Athinoula A. Martinos Center for Biomedical Imaging, Massachusetts General Hospital, Building 149, Room 2301, 13th Street, Charlestown, MA 02129, USA

David E. Sosnovik: sosnovik@nmr.mgh.harvard.edu

Abstract

Pathology in the heart can be examined at several scales, ranging from the molecular to the macroscopic. Traditionally, fluorescence-based techniques such as flow cytometry have been used to study the myocardium at the molecular, cellular, and microscopic levels. Recent advances in magnetic resonance imaging (MRI), however, have made it possible to image certain cellular and molecular events in the myocardium noninvasively in vivo. In addition, diffusion MRI has been used to image myocardial fiber architecture and microstructure in the intact heart. Diffusion MRI tractography, in particular, is providing novel insights into myocardial microsctructure in both health and disease. Recent developments have also been made in fluorescence imaging, making it possible to image fluorescent probes in the heart of small animals non-invasively in vivo. Moreover, techniques have been developed to perform in vivo fluorescence tomography of the mouse heart. These advances in MRI and fluorescence imaging allow events in the myocardium to be imaged at several scales linking molecular changes to alterations in microstructure and microstructural changes to gross function. A complete and integrated picture of pathophysiology in the myocardium is thus obtained. This multiscale approach has the potential to be of significant value not only in preclinical research but, ultimately, in the clinical arena as well.

Keywords

MRI; Myocardium; Molecular imaging; Microstructure; Fluorescence; Diffusion MRI

Introduction

Characterizing changes in the myocardium often requires evaluation across multiple spatial scales. Recently developed molecular imaging techniques have and are continuing to provide insights into cellular and subcellular aspects of cardiac disease [1, 2]. New techniques are also being developed to measure the microstructural organization of the myocardium and elucidate the biological mechanisms that link cellular and whole-organ

Correspondence to: David E. Sosnovik, sosnovik@nmr.mgh.harvard.edu.

pathology [3]. At the other end of the scale, macroscopic imaging methods to acquire global information concerning overall organ health and function continue to be refined [4]. In the current article, we review recent advances in molecular and microstructural imaging of the myocardium and focus particularly on the use of fluorescence molecular tomography (FMT) and magnetic resonance imaging (MRI).

MRI has been traditionally used to image macroscopic phenomena such as contraction, flow, and infarction in the myocardium [5]. During the last decade, however, several molecular MRI contrast agents have been developed to image apoptosis, necrosis, inflammation, peroxidase activity, and angiogenesis in the myocardium [6–8]. While the principal challenge in molecular MRI has been the development of novel imaging agents [9], the principal breakthroughs in fluorescence imaging have been in probe chemistry as well as hardware and image reconstruction algorithms [10]. The development of near-infrared fluorochromes has allowed structures 3 to 4 cm deep to be imaged [11, 12]. Tomographic systems with source-detector configurations similar to those of X-ray computed tomography have been developed [13], and reconstruction algorithms which account for the scattering of light by tissue have been introduced [11, 14]. Thus, molecular and cellular events in the myocardium of small animals can now be imaged noninvasively with FMT.

Microstructural imaging of the myocardium is most frequently performed with diffusion-encoded MRI [3]. This allows the orientation of myofiber tracts and sheets to be resolved non-destructively in three dimensions. Several diffusion-encoding techniques have been described, and the reader interested in a technical description of these is referred to several recent reviews [15–17]. In this article, we will focus on microstructural imaging with the recently developed diffusion spectrum MRI tractography (DSI) technique. This technique allows myofiber tracts to be resolved and provides a readout of myocardial organization between that of the cell and the whole organ [3]. Both MRI and fluorescence imaging have thus evolved from their traditional niches and now provide the opportunity for multiscale imaging of cells, fibers, and physiology in the myocardium.

Molecular MRI

Imaging Probes

Molecular MRI of the myocardium can be performed with magnetic nanoparticles (MNPs) or gadolinium-based (Gd) agents. MNPs, such as cross-linked iron oxide (CLIO), are small (less than 50 nm in size), consist of a superparamagnetic iron oxide core, have high magnetic relaxivities, are highly stable, and are coated with a biologically inert material such as dextran [18]. Several formulations of MNPs circulate in the blood stream for an extended period, making them ideal for imaging of the cardiovascular system. Unmodified MNPs have a circulatory half-life of approximately 12 h in mice, but conjugation of a ligand to the particles can decrease the half-life to less than 3 h [7, 19], an advantage as acute processes within the myocardium can be imaged with less background signal. In acute injury, the capillary membrane becomes hyperpermeable, allowing MNPs to reach the interstitial space rapidly in large amounts. MNPs are able to cross normal capillary membranes, although this process can take several hours. Once in the interstitial space, the inert nature of certain MNPs allows them to avoid non-specific binding and thus bind specifically to the target of interest on the cardiomyocyte surface. Once bound to the cell surface, these targeted MNPs are internalized and aggregate in lysosomes, forming a nano-assembly of particles with a higher transverse relaxivity (r2*) and hence higher detectability [20].

Gd-based molecular MRI probes for myocardial imaging can be either small chelates or large nanoparticulate constructs (i.e., micelles, liposomes, quantum dots) [21]. Large

constructs can be used to image endothelial targets in the myocardium but cannot easily penetrate into the interstitial space. In addition, these large constructs are frequently taken up non-specifically in the complex environment of the interstitial space and are thus not suited to targeted molecular MRI of the interstitium or the cardiomyocyte surface. Small Gd chelates do not suffer from these issues but have far lower sensitivities (micro-molar vs. nanomolar) and can thus only be used to image highly expressed targets in the myocardium such as collagen [22].

Molecular MRI of Cardiomyocyte Apoptosis

The largest experience with molecular MRI in the myocardium has been in the imaging of apoptosis. An apoptosis sensing MNP called annexin (Anx)CLIO-Cy5.5 has been developed which provides the ability to visualize the probe with both MRI and fluorescence. The Anx portion of the probe binds to phosphatidylserine, a phospholipid component that is usually kept on the inside of the cell membrane but becomes exposed on the cell surface once apoptosis has begun. The CLIO portion of the MNP provides the MR readout while the Cy5.5 fluorochrome allows for the localization of probe at a microscopic level with near-infrared fluorescence (NIRF). AnxCLIO-Cy5.5 has been able to image cardiomyocyte apoptosis in both ischemic injury and heart failure [7–9]. The extent of apoptosis and hence the uptake of the agent in acute ischemia was influenced significantly by the severity of injury (Fig. 1). In mild–moderate injury, AnxCLIO-Cy5.5 uptake was confined to the midmyocardium. In mice with severe injury, the uptake of the agent was more transmural. NIRF microscopy confirmed that the probe was primarily bound to the cell surface of morphologically intact cardiomyocytes (Fig. 1). This suggests that CM apoptosis begins in the midmyocardium and spreads transmurally as the severity of injury increases. Of note, the imaging in this study was performed 4 h after ischemic injury, during which apoptosis is maximal and well before the myocardium becomes infiltrated with inflammatory cells (see below).

Macrophage Infiltration of Infarcted Tissue

The myocardium becomes heavily infiltrated with proteolytic macrophages 24 to 72 h after an infarction [23]. MNPs are actively engulfed by macrophages and can be used to image cardiac inflammation associated with ischemic heart disease. Both conventional gradient-echo techniques and off-resonance MRI techniques have been used to image macrophage infiltration 72 to 96 h after myocardial infarction [10, 24]. MNPs have high transverse relaxivity, significantly reducing the intensity of the MRI signal in T2*-weighted gradient-echo sequences (Fig. 2). Thus, macrophages that have taken up MNPs produce signal hypointensity. A positive-contrast off-resonance technique has been tested in the identical infarct model (Fig. 2), but this technique was less sensitive and did not display the same linear relationship seen with the conventional gradient-echo approach [24]. Regardless, off-resonance and other positive-contrast approaches demonstrate the range and flexibility of contrast mechanisms available to molecular MRI.

Myeloperoxidase Activity Imaged with an Activatable MRI Agent

Macrophages infiltrating infarcted myocardium secrete numerous degradative and cytotoxic enzymes including myeloperoxidase (MPO). In the presence of MPO, serotonin is oxidized, causing a Gd-serotonin chelate to form dimers and oligomers with higher relaxivity [25]. This change in magnetic relaxivity can be exploited to image MPO activity in infarcted myocardium [26]. Activation of the probe causes an increase in r1 and, hence, signal hyperintensity of T1-weighted images. Knockout mice that were either heterozygous or homozygous for the MPO gene, however, did not show the same signal changes (Fig. 2d–f). This result confirmed the specificity of the contrast agent for MPO and demonstrated the utility of MRI for imaging enzymatic activity in vivo.

Imaging the Loss of Cell Viability

Delayed Gd enhancement is frequently used to assess myocardial viability. The cellular visualization of Gd distribution in infarcted myocardium, however, has proven difficult. The conjugation of conventional fluorochromes to small Gd chelates usually changes the pharmacokinetics of the probe significantly. However, the recent development of a novel fluorescent small Gd chelate (gadolinium diethylenetriamine pentaacetic acid nitrobenzoxadiazole, Gd-DTPA-NBD) has produced a Gd chelate that remains suitable for delayed enhancement imaging of the myocardium (Fig. 3a–c) [7]. NBD is small, carries no charge, and has only a small protein binding potential. In addition, Gd-DTPA-NBD can be detected by MRI, fluorescence imaging, and immunohistochemistry. Initial testing of the probe was performed in a mouse model of myocardial infarction. Gd-DTPA-NBD showed the typical pattern of delayed enhancement by MRI, which corresponded well to fluorescence reflectance imaging of the agent. Immunohistochemistry confirmed that the chelate accumulated only in regions of necrosis and cell rupture, where the volume fraction of the extracellular space had increased [7].

Myocardial Angiogenesis After Infarction

Angiogenesis is part of the early healing response of the myocardium to infarction. Recently, the development of a cyclic Asn-Gly-Arg (cNGR)-labeled paramagnetic quantum dot (pQDs) was reported and shown to bind to CD13, a zinc-dependent aminopeptidase that is upregulated during angiogenesis [27]. Infarcted mice injected with this agent 7 days after coronary artery ligation showed strong negative contrast in the injured myocardium (Fig. 3d). Ex vivo validation with two-photon laser scanning microscopy revealed a strong colocalization of the cNGR-pQDs probe with vascular endothelial cells. Current research is being done to couple this ligand to MNPs in order to develop a probe that may be more clinically applicable.

Imaging Fibrosis in Healed Infarcts

In addition to angiogenesis, the healing infarct is characterized by collagen deposition to form a scar. Healed infarcts are thus characterized by collagen-rich scars, which oppose expansion and rupture of the infarct [28]. To quantify the development of fibrosis, a Gd-based MR contrast agent with a peptide specific for type I collagen has recently been developed [29]. After injection of the probe, serial imaging of chronically infarcted mice was performed using a T1-weighted inversion recovery sequence. This revealed that the control probe was characterized by delayed washout and enhancement but, nevertheless, had fully washed out of the infarct within 40 min of injection. The active collagen binding probe, however, was retained in the infarct and allowed collagen content of the infarct scar to be clearly visualized (Fig. 3e) [29].

Dual-Contrast Imaging

Several approaches are being developed to image more than one molecular imaging agent simultaneously. These include the use of fluorine MRI and novel endogenous contrast mechanisms [30–33]. It was also recently shown that cardiomyocyte necrosis and apoptosis can be imaged simultaneously in vivo using a dual-contrast approach [7]. The probe AnxCLIO-Cy5.5 is taken up in both apoptotic cells (which express phosphatidylserine on the outer membrane surface) and necrotic cells, making it a marker for composite cell death (Fig. 4). The dual use of delayed enhancement imaging with Gd-DTPA-NBD, however, allowed the uptake of AnxCLIO-Cy5.5 due to apoptosis and necrosis to be differentiated [7]. Areas of myocardium showing uptake of AnxCLIO-Cy5.5 were classified as apoptotic, while those showing the uptake of both probes were labeled as necrotic. Using this approach in a mouse model, it was shown that large areas of apoptotic (but potentially viable)

myocardium are present in the mid-myocardium within the first few hours of ischemia–reperfusion injury [7].

Fluorescence Imaging of the Myocardium

The attributes of fluorescence imaging are highly complementary to those of MRI. The sensitivity and multispectral nature of fluorescence imaging have made it an indispensible tool for in vitro imaging. Current schemes to perform fluorescence imaging in vivo, however, are usually invasive and limited to surface imaging. For fluorescence imaging of organs deep within the body to be performed noninvasively, light at both the excitation and emission wavelengths must be able to penetrate tissue without being excessively attenuated. Thus, organic fluorochromes in the near-infrared spectrum must be used for noninvasive fluorescence imaging of deep structures [12]. Unlike X-ray radiation that is only absorbed, the propagation of light in tissue is diffuse in nature and is a function of both scattering and absorption [12, 13].

Planar Transillumination Fluorescent Imaging

Some of the first noninvasive in vivo fluorescence imaging of the myocardium focused on the detection of macrophage infiltration in mice with healing myocardial infarctions [10]. Mice injected with CLIO-Cy5.5, a cross-linked iron oxide probe with an attached Cy5.5 fluorochrome, showed robust nanoparticle accumulation 96 h after infarction (Fig. 5). Fluorescence microscopy and immunohistochemistry confirmed that the probe was endocytosed by macrophages in the injured tissue. While planar fluorescence imaging is of major value, it is not depth-resolved. This creates challenges in accurately quantifying the fluorescence signal and ensuring that it is arising solely from the organ of interest [10]. FMT of near-infrared fluorochromes in the heart overcomes some of these limitations and has been actively pursued.

Fluorescent Molecular Tomography of Macrophage Infiltration

Several generations of FMT systems have been developed [10, 13]. FMT of the myocardium was first performed on second-generation systems that required the mice to be immersed in an intralipid solution. Current third-generation systems employ 360° ring detector configurations and no longer require the use of optical matching media. FMT of the myocardium was also first performed in infarcted mice, injected with the CLIO-Cy5.5 nanoparticle, and imaged 96 h after infarction (Fig. 6) [10]. Analogous to the signal seen in T2*-weighted MRI, the FMT signal increased linearly with the dose of CLIO-Cy5.5 injected. In a subsequent study, FMT was used to image a near-infrared probe that can be activated by proteases, principally cathepsins, in healing infarcts [34]. Healing infarcts attract a large number of activated macrophages, which in turn produce copious amounts of active cathepsins. These enzymes then cleave a recognition site in the linker portion of the probe between discrete Cy5.5 molecules, allowing for the separation of tightly spaced fluorochromes that were previously quenched in the inactive state [35]. FMT of the myocardium has become an extremely valuable research tool in the preclinical setting. However, even in the near-infrared portion of the spectrum, significant absorption and scattering of light limit penetration to a few centimeters. This limits fluorescence imaging in humans to superficial structures or invasive techniques. Thus, fluorescence imaging of the human heart will likely require surgical or catheter-based approaches for the foreseeable future.

Microstructural Imaging of the Myocardium

Cardiac mechanics is greatly affected by the microstructure of the myocardium. Specifically, the orientation of myofiber tracts in the myocardium plays a central role in the contraction of

the ventricle. Seminal studies using histology showed that the heart is composed of an array of crossing helical myofibers [36, 37]. MRI has the ability to image these muscle tracts by measuring the diffusion of water molecules within the tissue. MR diffusion tensor imaging (DTI) has been implemented to approximate the three-dimensional fiber structure of the heart [38] and has been successfully used to quantify infarct healing after ischemic injury in animal models [39, 40]. Differences were seen in mean diffusivity (MD), fractional anisotropy (FA), and fiber orientation between healthy and infarcted regions. MD is a measure of how freely water diffuses and is reduced by the organized structure of the myofibers and connective tissue network in normal myocardium. FA is a measure of whether water diffuses preferentially in one direction. Patients and animals with acute infarcts have shown an increase in MD and decrease in FA. These scalar measurements of myocardial microstructure have the potential to play an important role in the ongoing development and application of microstructural imaging in the myocardium.

Diffusion MR Tractography Techniques

DTI can be used to derive several important vector measurements of myocardial microstructure. Perhaps the most important of these is the primary eigenvector, which indicates the principal direction of water diffusion. The primary eigenvectors in a 3D field can be integrated into streamlines, which indicate the course of myofiber tracts. While this has been extensively performed in the brain [41], the application of this technique to the myocardium has been relatively recent. A further advance in the field of microstructural imaging has been the development of DSI [3]. While complex and time-consuming, DSI is considered to be the gold standard of all the diffusion imaging techniques that sample diffusion space (or q-space) with high angular resolution [42–44]. Every voxel in the spatial (x, y, z) domain of a DSI acquisition has its own 3D diffusion or q-space associated with it (Fig. 7). Since water diffuses primarily along the long axis of myofibers, the Fourier transformation of q-space produces a probability density function (PDF), where the local maxima represent the directions of fiber orientation within each voxel (Fig. 7). The reader interested in more information on the physical basis of DTI, DSI, and other diffusion imaging techniques is referred to a recent review [16].

Myofiber Tractograms and Ventricular Architecture

Myofibers form a series of crossing spiral structures in healthy myocardium where the helix angle varies from a right-handed helix in the subendocardium to a left-handed helix in the subepicardium [36, 37]. In a recent DSI tractography study of rat hearts, a smooth transition in fiber orientation from epicardium to endocardium was seen (Figs. 8 and 9a–c) [3, 16]. In infarcted hearts, however, myofiber architecture was severely disrupted (Fig. 9d–f). Numerous residual myofibers were present within the infarcts, forming a mesh-like network of orthogonal fibers in the basal and septal portions of the infarcted region. Perpendicular fibers within this area often lay in direct contact with each other, creating nodes of myofiber contact [3]. The implications of such a pattern remain to be determined, but it is possible these fibers provide greater structural support while increasing the risk of the formation of lethal reentrant arrhythmias.

Efforts to perform DTI in the heart in vivo have been made for over a decade [38]. While in vivo imaging of 3D fiber architecture remains a challenge, 2D DTI in humans has been described [45, 46]. In vivo 2D DTI in patients with recent infarcts showed an increase in mean diffusivity, a decrease in FA, and a loss of right-handed (subendocardial) fibers in the infarct zone [47]. A follow-up study in these patients demonstrated the potential of DTI to resolve serial changes in myocardial microstructure in both the infarct and the remote zone: An increase in right-handed fibers in the remote zone correlated with better function [48]. These studies demonstrate the potential of microstructural imaging in humans and the value

of correlating microstructural changes with functional remodeling. Tractography of the human heart in vivo remains experimental. Nonetheless, a method for the 3D interpolation and reconstruction of fiber architecture in the left ventricle from sparse DTI datasets in normal volunteers has recently been described [49]. Further work, however, will be needed to bring diffusion tractography into the clinical mainstream.

Conclusion

The role of both MRI and fluorescence imaging in studies of myocardial injury and remodeling continues to grow. While fluorescence imaging is extremely sensitive and multispectral in nature, molecular MRI provides high-resolution images that can correlate myocardial structure and function. The ability to combine molecular and microstructural imaging is particularly appealing since it allows events at the subcellular level to be linked to gross changes of the heart. Further efforts to refine both MRI and optical instrumentation, as well as probes for multi-modality molecular imaging, are likely to further improve this multiscale approach. The characterization of the myocardium with noninvasive imaging techniques has thus moved well beyond traditional macroscopic indices and into the era of multiscale measurement. Molecular and microstuctural imaging are already playing an important role in preclinical investigation and have the potential to play an equally important role in the clinical arena as well.

Acknowledgments

Dr. Sosnovik has been funded in part by the following National Institutes of Health grant: R01 HL093038.

References

1. Nahrendorf M, Sosnovik DE, French BA, Swirski FK, Bengel F, Sadeghi MM, et al. Multimodality cardiovascular molecular imaging, part II. Circulation Cardiovascular Imaging. 2009; 2(1):56–70. [PubMed: 19808565]
2. Sosnovik DE, Nahrendorf M, Weissleder R. Molecular magnetic resonance imaging in cardiovascular medicine. Circulation. 2007; 115(15):2076–2086. [PubMed: 17438163]
3. Sosnovik DE, Wang R, Dai G, Wang T, Aikawa E, Novikov M, et al. Diffusion spectrum MRI tractography reveals the presence of a complex network of residual myofibers in infarcted myocardium. Circulation Cardiovascular Imaging. 2009; 2 (3):206–212. [PubMed: 19808594]
4. Assomull RG, Pennell DJ, Prasad SK. Cardiovascular magnetic resonance in the evaluation of heart failure. Heart. 2007; 93(8):985–992. [PubMed: 17639116]
5. Lockie T, Nagel E, Redwood S, Plein S. Use of cardiovascular magnetic resonance imaging in acute coronary syndromes. Circulation. 2009; 119(12):1671–1681. [PubMed: 19332480]
6. Korngold EC, Jaffer FA, Weissleder R, Sosnovik DE. Noninvasive imaging of apoptosis in cardiovascular disease. Heart Failure Reviews. 2008; 13(2):163–173. [PubMed: 18074226]
7. Sosnovik DE, Garanger E, Aikawa E, Nahrendorf M, Figuiredo JL, Dai G, et al. Molecular MRI of cardiomyocyte apoptosis with simultaneous delayed-enhancement MRI distinguishes apoptotic and necrotic myocytes in vivo: Potential for midmyocardial salvage in acute ischemia. Circulation Cardiovascular Imaging. 2009; 2(6):460–467. [PubMed: 19920044]
8. Sosnovik DE, Schellenberger EA, Nahrendorf M, Novikov MS, Matsui T, Dai G, et al. Magnetic resonance imaging of cardiomyocyte apoptosis with a novel magneto-optical nanoparticle. Magnetic Resonance in Medicine. 2005; 54(3):718–724. [PubMed: 16086367]
9. Lanza GM, Winter P, Caruthers S, Schmeider A, Crowder K, Morawski A, et al. Novel paramagnetic contrast agents for molecular imaging and targeted drug delivery. Current Pharmaceutical Biotechnology. 2004; 5(6):495–507. [PubMed: 15579039]
10. Sosnovik DE, Nahrendorf M, Deliolanis N, Novikov M, Aikawa E, Josephson L, et al. Fluorescence tomography and magnetic resonance imaging of myocardial macrophage infiltration in infarcted myocardium in vivo. Circulation. 2007; 115 (11):1384–1391. [PubMed: 17339546]

11. Ntziachristos V, Ripoll J, Wang LV, Weissleder R. Looking and listening to light: The evolution of whole-body photonic imaging. Nature Biotechnology. 2005; 23(3):313–320.
12. Weissleder R, Ntziachristos V. Shedding light onto live molecular targets. Natural Medicines. 2003; 9(1):123–128.
13. Graves EE, Ripoll J, Weissleder R, Ntziachristos V. A submillimeter resolution fluorescence molecular imaging system for small animal imaging. Medical Physics. 2003; 30(5):901–911. [PubMed: 12772999]
14. Meyer H, Garofalakis A, Zacharakis G, Psycharakis S, Mamalaki C, Kioussis D, et al. Noncontact optical imaging in mice with full angular coverage and automatic surface extraction. Applied Optics. 2007; 46(17):3617–3627. [PubMed: 17514324]
15. Huang S, Sosnovik DE. Molecular and microstructural imaging of the myocardium. Curr Cardiovasc Imaging Rep. 2010; 3(1):26–33. [PubMed: 20689659]
16. Sosnovik DE, Wang R, Dai G, Reese TG, Wedeen VJ. Diffusion MR tractography of the heart. Journal of Cardiovascular Magnetic Resonance. 2009; 11:47. [PubMed: 19912654]
17. Kramer CM, Sinusas AJ, Sosnovik DE, French BA, Bengel FM. Multimodality imaging of myocardial injury and remodeling. Journal of Nuclear Medicine. 2010; 51(Suppl 1):107S–121S. [PubMed: 20395347]
18. Sosnovik DE, Nahrendorf M, Weissleder R. Magnetic nanoparticles for MR imaging: Agents, techniques and cardiovascular applications. Basic Research in Cardiology. 2008; 103 (2):122–130. [PubMed: 18324368]
19. Montet X, Montet-Abou K, Reynolds F, Weissleder R, Josephson L. Nanoparticle imaging of integrins on tumor cells. Neoplasia. 2006; 8(3):214–222. [PubMed: 16611415]
20. Taktak S, Sosnovik D, Cima MJ, Weissleder R, Josephson L. Multiparameter magnetic relaxation switch assays. Analytical Chemistry. 2007; 79(23):8863–8869. [PubMed: 17983206]
21. Uppal R, Caravan P. Targeted probes for cardiovascular MR imaging. Future Medicinal Chemistry. 2010; 2(3):451–470. [PubMed: 20539821]
22. Caravan P. Protein-targeted gadolinium-based magnetic resonance imaging (MRI) contrast agents: Design and mechanism of action. Accounts of Chemical Research. 2009; 42(7):851–862. [PubMed: 19222207]
23. Nahrendorf M, Swirski FK, Aikawa E, Stangenberg L, Wurdinger T, Figueiredo JL, et al. The healing myocardium sequentially mobilizes two monocyte subsets with divergent and complementary functions. The Journal of Experimental Medicine. 2007; 204(12):3037–3047. [PubMed: 18025128]
24. Farrar CT, Dai G, Novikov M, Rosenzweig A, Weissleder R, Rosen BR, et al. Impact of field strength and iron oxide nanoparticle concentration on the linearity and diagnostic accuracy of off-resonance imaging. NMR in Biomedicine. 2008; 21(5):453–463. [PubMed: 17918777]
25. Chen JW, Querol Sans M, Bogdanov A Jr, Weissleder R. Imaging of myeloperoxidase in mice by using novel amplifiable paramagnetic substrates. Radiology. 2006; 240(2):473–481. [PubMed: 16864673]
26. Nahrendorf M, Sosnovik D, Chen JW, Panizzi P, Figueiredo JL, Aikawa E, et al. Activatable magnetic resonance imaging agent reports myeloperoxidase activity in healing infarcts and noninvasively detects the antiinflammatory effects of atorvastatin on ischemia–reperfusion injury. Circulation. 2008; 117 (9):1153–1160. [PubMed: 18268141]
27. Oostendorp M, Douma K, Wagenaar A, Slenter JM, Hackeng TM, van Zandvoort MA, et al. Molecular magnetic resonance imaging of myocardial angiogenesis after acute myocardial infarction. Circulation. 2010; 121(6):775–783. [PubMed: 20124125]
28. Verjans JW, van de Borne SW, Hofstra L, Narula J. Molecular imaging of myocardial remodeling after infarction. Methods in Molecular Biology. 2011; 680:227–235. [PubMed: 21153384]
29. Caravan P, Das B, Dumas S, Epstein FH, Helm PA, Jacques V, et al. Collagen-targeted MRI contrast agent for molecular imaging of fibrosis. Angewandte Chemie (International Edin English). 2007; 46(43):8171–8173.
30. Huang TY, Liu YJ, Stemmer A, Poncelet BP. T2 measurement of the human myocardium using a T2-prepared transient-state TrueFISP sequence. Magnetic Resonance in Medicine. 2007; 57(5): 960–966. [PubMed: 17457877]

31. Waters EA, Chen J, Allen JS, Zhang H, Lanza GM, Wickline SA. Detection and quantification of angiogenesis in experimental valve disease with integrin-targeted nanoparticles and 19-fluorine MRI/MRS. Journal of Cardiovascular Magnetic Resonance. 2008; 10:43. [PubMed: 18817557]
32. Weber OM, Speier P, Scheffler K, Bieri O. Assessment of magnetization transfer effects in myocardial tissue using balanced steady-state free precession (bSSFP) cine MRI. Magnetic Resonance in Medicine. 2009; 62(3):699–705. [PubMed: 19572387]
33. Zun Z, Wong EC, Nayak KS. Assessment of myocardial blood flow (MBF) in humans using arterial spin labeling (ASL): feasibility and noise analysis. Magnetic Resonance in Medicine. 2009; 62(4):975–983. [PubMed: 19672944]
34. Nahrendorf M, Sosnovik DE, Waterman P, Swirski FK, Pande AN, Aikawa E, et al. Dual channel optical tomographic imaging of leukocyte recruitment and protease activity in the healing myocardial infarct. Circulation Research. 2007; 100(8):1218–1225. [PubMed: 17379832]
35. Mahmood U, Tung CH, Bogdanov A Jr, Weissleder R. Near-infrared optical imaging of protease activity for tumor detection. Radiology. 1999; 213(3):866–870. [PubMed: 10580968]
36. Streeter DD Jr, Spotnitz HM, Patel DP, Ross J Jr, Sonnenblick EH. Fiber orientation in the canine left ventricle during diastole and systole. Circulation Research. 1969; 24(3):339–347. [PubMed: 5766515]
37. Streeter DD Jr, Hanna WT. Engineering mechanics for successive states in canine left ventricular myocardium. II. Fiber angle and sarcomere length. Circulation Research. 1973; 33(6):656–664. [PubMed: 4762007]
38. Reese TG, Weisskoff RM, Smith RN, Rosen BR, Dinsmore RE, Wedeen VJ. Imaging myocardial fiber architecture in vivo with magnetic resonance. Magnetic Resonance in Medicine. 1995; 34(6): 786–791. [PubMed: 8598805]
39. Chen J, Song SK, Liu W, McLean M, Allen JS, Tan J, et al. Remodeling of cardiac fiber structure after infarction in rats quantified with diffusion tensor MRI. American Journal of Physiology Heart and Circulatory Physiology. 2003; 285(3):H946–H954. [PubMed: 12763752]
40. Strijkers GJ, Bouts A, Blankesteijn WM, Peeters TH, Vilanova A, van Prooijen MC, et al. Diffusion tensor imaging of left ventricular remodeling in response to myocardial infarction in the mouse. NMR in Biomedicine. 2009; 22 (2):182–190. [PubMed: 18780284]
41. Lazar M. Mapping brain anatomical connectivity using white matter tractography. NMR in Biomedicine. 2010; 23(7):821–835. [PubMed: 20886567]
42. Hagmann P, Jonasson L, Maeder P, Thiran JP, Wedeen VJ, Meuli R. Understanding diffusion MR imaging techniques: From scalar diffusion-weighted imaging to diffusion tensor imaging and beyond. Radiographics. 2006; 26(Suppl 1):S205–S223. [PubMed: 17050517]
43. Kuo LW, Chen JH, Wedeen VJ, Tseng WY. Optimization of diffusion spectrum imaging and q-ball imaging on clinical MRI system. Neuroimage. 2008; 41(1):7–18. [PubMed: 18387822]
44. Wedeen VJ, Wang RP, Schmahmann JD, Benner T, Tseng WY, Dai G, et al. Diffusion spectrum magnetic resonance imaging (DSI) tractography of crossing fibers. Neuroimage. 2008; 41(4): 1267–1277. [PubMed: 18495497]
45. Tseng WY, Reese TG, Weisskoff RM, Wedeen VJ. Cardiac diffusion tensor MRI in vivo without strain correction. Magnetic resonance in medicine: official journal of the Society of Magnetic Resonance in Medicine/Society of Magnetic Resonance in Medicine. 1999; 42(2):393–403. [PubMed: 10440965]
46. Gamper U, Boesiger P, Kozerke S. Diffusion imaging of the in vivo heart using spin echoes—considerations on bulk motion sensitivity. Magnetic resonance in medicine: official journal of the Society of Magnetic Resonance in Medicine/Society of Magnetic Resonance in Medicine. 2007; 57(2):331–337. [PubMed: 17260376]
47. Wu MT, Tseng WY, Su MY, Liu CP, Chiou KR, Wedeen VJ, et al. Diffusion tensor magnetic resonance imaging mapping the fiber architecture remodeling in human myocardium after infarction: Correlation with viability and wall motion. Circulation. 2006; 114(10):1036–1045. [PubMed: 16940196]
48. Wu MT, Su MY, Huang YL, Chiou KR, Yang P, Pan HB, et al. Sequential changes of myocardial microstructure in patients postmyocardial infarction by diffusion-tensor cardiac MR: correlation

with left ventricular structure and function. Circulation Cardiovascular imaging. 2009; 2(1):32–40. 36 p following 40. [PubMed: 19808562]

49. Toussaint N, Sermesant M, Stoeck CT, Kozerke S, Batchelor PG. In vivo human 3D cardiac fibre architecture: Reconstruction using curvilinear interpolation of diffusion tensor images. Med Image Comput Comput Assist Interv. 2010; 13(Pt 1):418–425. [PubMed: 20879258]

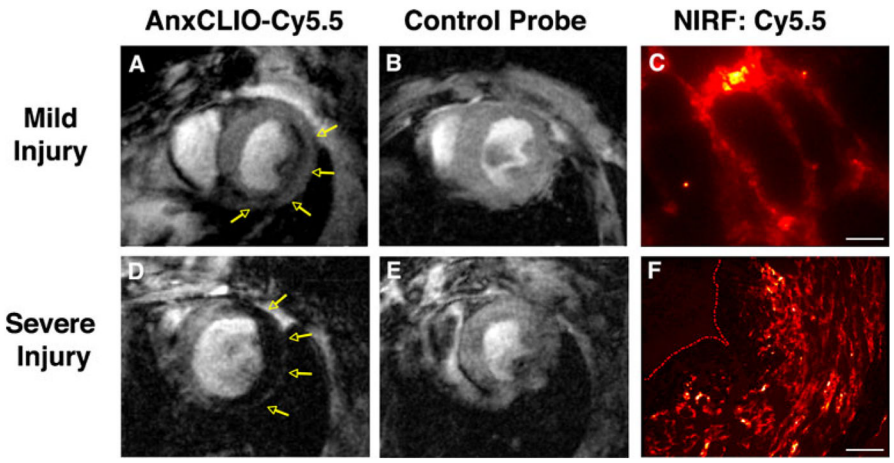

Fig. 1.

Molecular MRI of cardiomyocyte apoptosis with AnxCLIO-Cy5.5. a In mice with mild–moderate injury, the uptake of AnxCLIO-Cy5.5 is confined to the midmyocardium and b no uptake of the control probe is seen. d In mice with severe injury, the uptake of AnxCLIO-Cy5.5 is transmural and e minimal retention of the control probe is seen. MRI in this study was performed 4 h after ischemia–reperfusion injury, which is significantly earlier than previous studies with radiolabeled annexin. The fluorochrome on the agent allows the cellular distribution of AnxCLIO-Cy5.5 to be confirmed with fluorescence microscopy (high magnification in c, scale bar represents 20 m; low magnification in f, scale bar represents 80 m); reproduced with permission from [7]

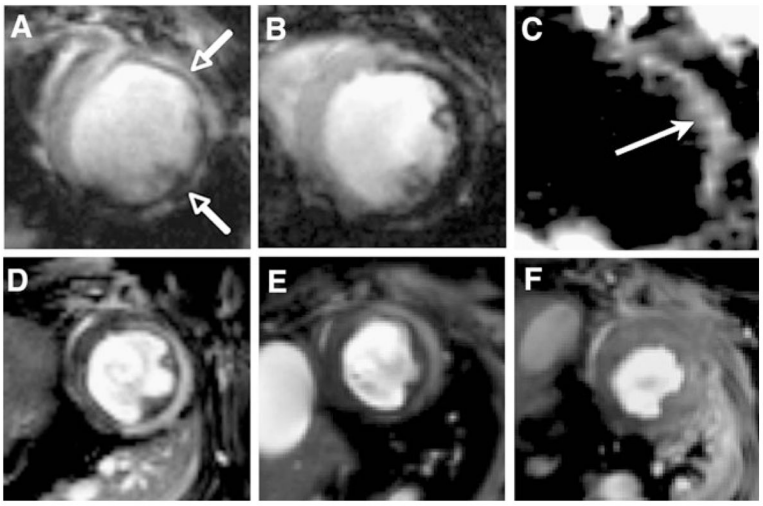

Fig. 2.

Molecular MRI of inflammation in healing myocardial infarcts. a–c Direct imaging of infiltrating macrophages. T2*-weighted images of mice 96 h after infarction and the intravenous injection of 3 mg iron per kg (a) or 20 mg iron per kg (b) of CLIO-Cy5.5. T2*-weighted imaging produces negative contrast enhancement in the injured myocardium (open arrows); reproduced with permission from [10]. c Off-resonance imaging of iron oxide accumulation within the macrophages infiltrating infarcted myocardium produces positive contrast (solid arrow); reproduced with permission from [24]. d, e Imaging of enzymes produced by the infiltrating macrophages. A myeloperoxidase activatable Gd chelate has been injected into mice with healing infarcts. d The chelate is activated by myeloperoxidase in the infarct producing positive contrast. e Only mild signal enhancement is seen in a heterozygous myeloperoxidase mouse, and f no enhancement is seen in the homozygous knockout mouse. Reproduced with permission from [26]

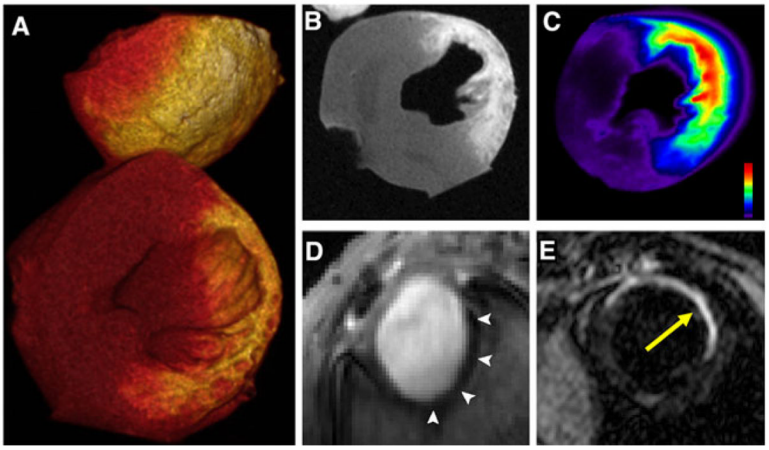

Fig. 3.

Molecular imaging of infarct evolution. a–c Loss of cardiomyocyte viability in acute infarction detected with delayed enhancement of Gd-DTPA-NBD in a heart excised 20 min after injection of the probe. Loss of cell membrane integrity expands the extracellular space leading to accumulation of the agent. a Volume rendered 3D MRI, b 2D short-axis reconstruction at midventricular level, and c fluorescent reflectance imaging. The accumulation of Gd-DTPA-NBD is well resolved with both MRI and fluorescence imaging. Reproduced with permission from [7]. d Angiogenesis in subacute healing infarcts: short-axis gradient-echo image of an infarcted mouse injected with integrin-sensing and Gd-loaded quantum dots (cNGR-pQDs). The r1/r2 ratio of the quantum dot differs significantly from small Gd chelates, producing negative enhancement (arrows); reproduced with permission from [27]. e Scar formation in chronic infarcts: MRI of myocardial fibrosis in mice with chronic infarcts injected with a collagen-targeted contrast agent (yellow arrow); reproduced with permission from [29]

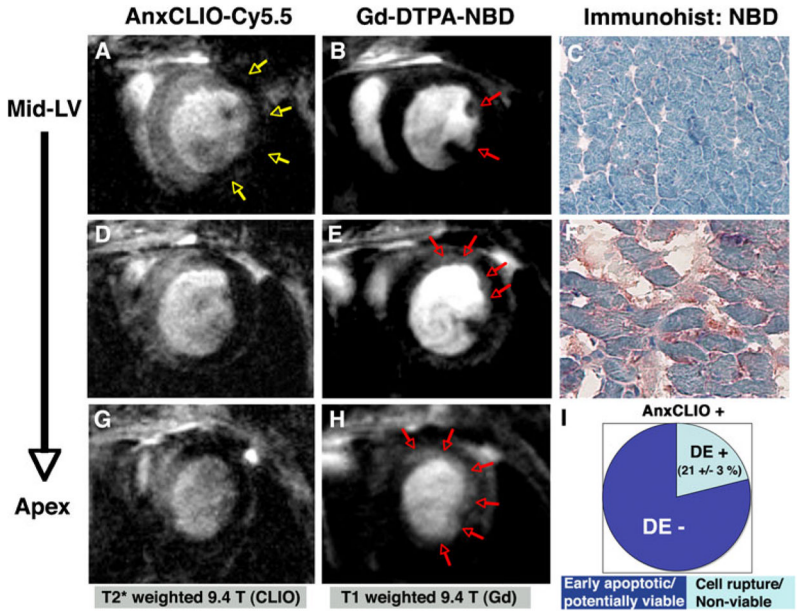

Fig. 4.

Dual molecular MRI of cardiomyocyte apoptosis and necrosis. To distinguish between apoptotic and necrotic tissue, both AnxCLIO-Cy5.5 MRI (a, d, g) and delayed enhancement MRI of Gd-DTPA-NBD (b, e, h) are required. Images from the same animal are shown in a–h. Images at three slice locations are shown, moving progressively from the midventricular level (a, b) to the left ventricular apex (g, h). AnxCLIO-Cy5.5 was administered immediately after reperfusion and imaged after 4 h, while Gd-DTPA-NBD was administered after the T2*-weighted imaging was completed and imaged 10–30 min after injection. Only a small area in the subendocardium of the lateral wall shows delayed enhancement at the midventricular level (red arrows, b). The extent of delayed enhancement increases in the more apical slices (red arrows) and is quite extensive at the apex. Immunohistochemistry for Gd-DTPA-NBD confirms the absence or presence of probe uptake in the uninjured septum (c) and antero-apical wall (f). Within 4 h of reperfusion, the majority of myocardium with accumulation of AnxCLIO-Cy5.5 does not yet show delayed enhancement of Gd-DTPA-NBD (i). These results suggest a large amount of apoptotic but potentially viable and salvageable myocardium is thus present. Reproduced with permission from [7]

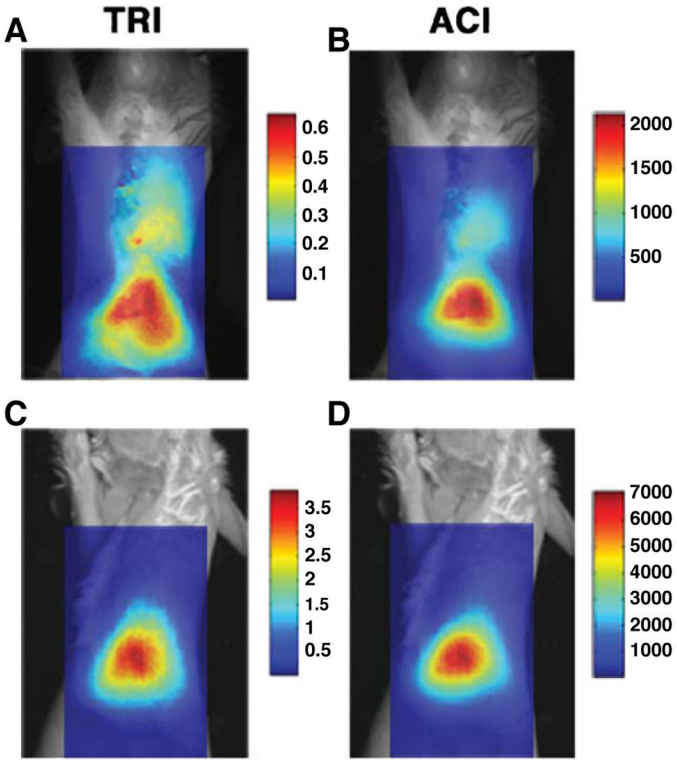

Fig. 5.

Planar fluorescence imaging of near-infrared fluorochromes. An infarcted mouse (a, b) and a sham-operated mouse (c, d) have been injected with CLIO-Cy5.5. The probe is taken up by macrophages infiltrating the healing infarct and can be imaged with fluorescence. The fluorescence images have been superimposed over white light images and two different postprocessing schemes have been used: TRI transillumination ratio image and ACI attenuation corrected image. While substantial hepatic uptake of CLIO-Cy5.5 is seen in both mice due to clearance of the probe in the liver, thoracic uptake of the agent is seen only in infarcted mice. Reproduced with permission from [10]

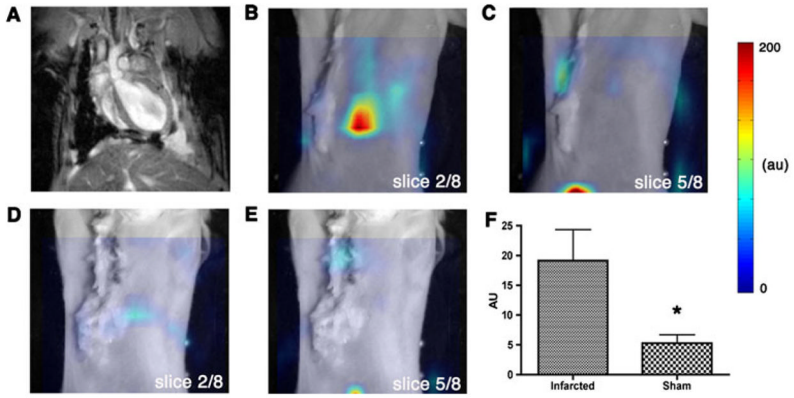

Fig. 6.

FMT of myocardial macrophage infiltration in vivo. Reconstructed coronal slices from the 3D FMT dataset have been superimposed over white light images of infarcted and control mice. Slices 2–4 in the FMT dataset intersected the heart, while slices 5–8 passed posterior to it. Long axis MRI in an infarcted mouse (a) corresponds to slice 2 from the fluorescence dataset of the same animal (b). As expected, c slice 5 showed only minor thoracic signal as this slice was posterior to the heart. The corresponding slices of a sham-operated mouse (d, e) also showed minimal thoracic uptake. Accumulation of the CLIO-Cy5.5 in the liver appears in the posterior slices of both the infarcted (c) and sham-operated (e) mice. f Depth-resolved fluorescence intensity in the heart was significantly greater (*$p<0.05$) in infarcted mice versus sham-operated. Reproduced with permission from [10]

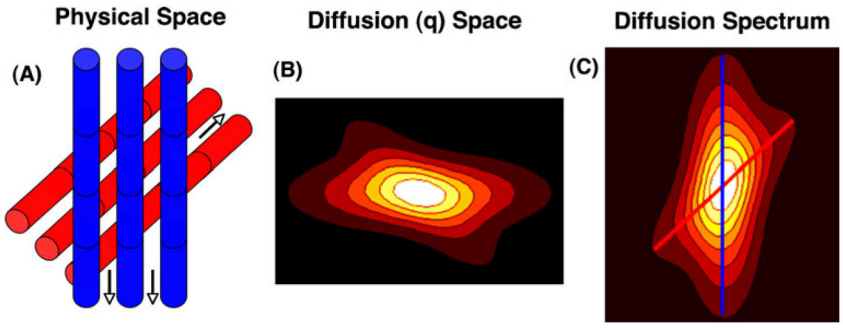

Fig. 7.

Basic principles of DSI tractography. a Water diffuses along the direction of myofibers (arrows). b Diffusion or q-space is sampled by measuring signal intensity during the application of many diffusion-encoding gradients or q-vectors. c Fourier transformation of q-space produces a PDF in which the local maxima represent the axes of the corresponding fiber orientations (blue and red lines). 3D myofiber tractograms are produced by the integration of the local maxima in the orientation density function into coherent streamlines. Diffusion tensor tractography works along similar principals. The primary eigenvector of the tensor indicates that the principal direction of diffusion and a 3D field of eigenvectors can be integrated into myofiber streamlines. Reproduced with permission from [16]

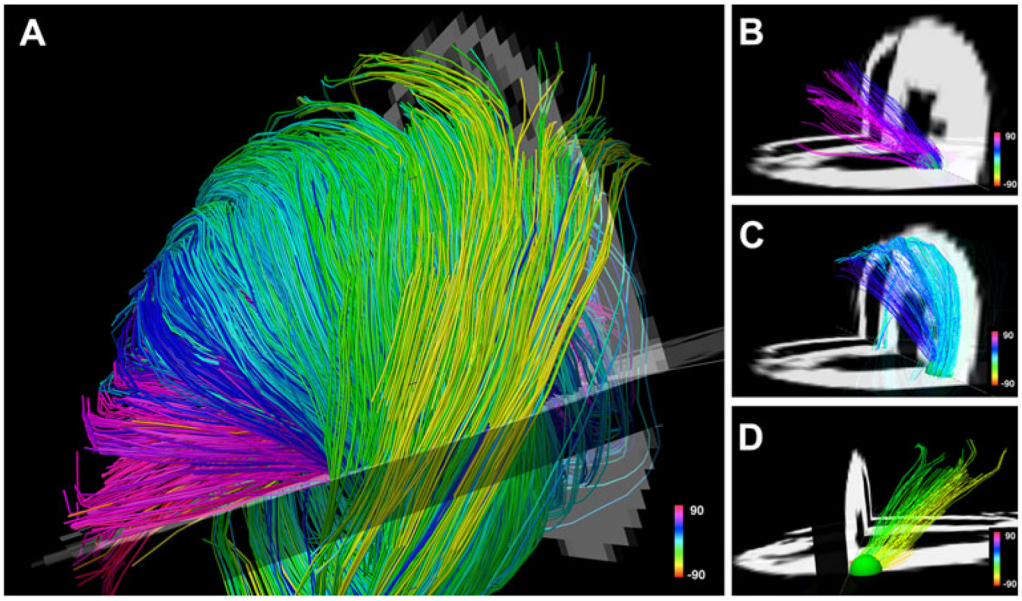

Fig. 8.
Myofiber architecture in a normal rat heart. The myofiber tracts have been generated ex vivo with the DSI technique. The fibers are color-coded by the spiral or helix angle they make with the ventricle. a The crossing helical architecture of the myocardium is easily seen. Only those fibers intersecting a spherical region-of-interest are displayed in b–d. Myofiber tracts in the subendocardium (b, pink to navy blue representing positive helix angles) and in the subepicardium (d, green yellow representing negative helix angles) have orthogonal helix angles and pass over each other in different transmural planes. c The fibers in the midmyocardium have a zero helix angle and are thus circumferential in orientation. Reproduced with permission from [16]

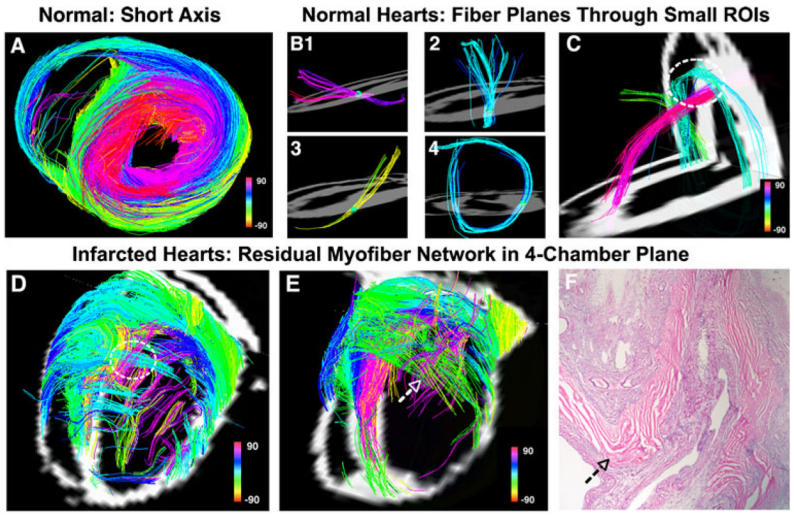

Fig. 9.

Comparison of normal and infarcted myofiber architecture. Rat hearts have been imaged ex vivo and are color-coded by helix angle. A normal rat heart is shown in a–c. a Short-axis view of the left ventricle reveals the transmural variation in myofiber helix angle. Fiber architecture is more clearly seen when only those fibers intersecting a small spherical region-of-interest are displayed. The fibers in (b, 1–3) are being viewed from the lateral wall and in (b, 4) from the apex. Myofibers in the midmyocardium are circumferential, while those in the subendocardium and subepicardium are angled and orthogonal to each other. c Again illustrates the presence of a network of orthogonal myofibers (subendocardial pink and midmyocardial blue) in distinct transmural planes (dashed circle). d, e Two infarcted rat hearts show severe perturbation of myofiber architecture in the anterolateral wall. The dashed white circle in d shows orthogonal myofibers making contact with each other in the same plane (compare to normal heart in c). The arrows in e and f mark the locations of nodes of orthogonal myofiber contact in the same heart. f The majority of the infarct is infiltrated with scar tissue (dargpurple color), while the residual myofibers appear bright pink. Reproduced with permission from [3]